High-Gain On-Chip Antenna Design on Silicon Layer With Aperture Excitation for Terahertz Applications

Mohammad Alibakhshikenari, *Member, IEEE*, Bal S. Virdee, *Senior Member, IEEE*, Mohsen Khalily, *Senior Member, IEEE*, Chan H. See, *Senior Member, IEEE*, Raed Abd-Alhameed, *Senior Member, IEEE*, Francisco Falcone, *Senior Member, IEEE*, Tayeb A. Denidni, *Fellow, IEEE*, and Ernesto Limiti, *Senior Member, IEEE*

***Abstract*—This letter investigates the feasibility of designing a high gain on-chip antenna on silicon technology for subterahertz applications over a wide-frequency range. High gain is achieved by exciting the antenna using an aperture fed mechanism to couple electromagnetics energy from a metal slot line, which is sandwiched between the silicon and polycarbonate substrates, to a 15-element array comprising circular and rectangular radiation patches fabricated on the top surface of the polycarbonate layer. An open ended microstrip line, which is orthogonal to the metal slot-line, is implemented on the underside of the silicon substrate. When the open ended microstrip line is excited it couples the signal to the metal slot-line which is subsequently coupled and radiated by the patch array. Measured results show the proposed on-chip antenna exhibits a reflection coefficient of less than −10 dB across 0.290–0.316 THz with a highest gain and radiation efficiency of 11.71 dBi and 70.8%, respectively, occurred at 0.3 THz. The antenna has a narrow stopband between 0.292 and 0.294 THz. The physical size of the presented subterahertz on-chip antenna is 20 × 3.5 × 0.126 mm^3.**

***Index Terms*—Coupling feeding mechanism, high gain, silicon technology, terahertz (THz) on-chip antenna, terahertz applications, wide- frequency range.**

Manuscript received June 19, 2020; revised July 10, 2020; accepted July 17, 2020. Date of publication July 21, 2020; date of current version September 3, 2020. This work was supported in part by RTI2018-095499-B-C31, funded by Ministerio de Ciencia, Innovacion y Universidades, Gobierno de Espana (MCIU/AEI/FEDER,UE), and Innovation Programme under Grant agreement H2020-MSCA-ITN-2016 SECRET-722424, and in part by U.K. EPSRC under Grant EP/E022936/1. *(Corresponding author: Mohammad Alibakhshikenari.)*

Mohammad Alibakhshikenari and Ernesto Limiti are with the Electronic Engineering Department, University of Rome “Tor Vergata,” 00133 Rome, Italy (e-mail: alibakhshikenari@ing.uniroma2.it; imiti@ing.uniroma2.it).

Bal S. Virdee is with the Center for Communications Technology, London Metropolitan University, N7 8DB London, U.K. (e-mail: b.virdee@londonmet.ac.uk).

Mohsen Khalily is with the Institute for Communication Systems (ICS), Home of 5G Innovation Centre (5GIC), University of Surrey, GU2 7XH Guildford, U.K. (e-mail: m.khalily@surrey.ac.uk).

Chan H. See was with the School of Engineering, University of Bolton, BL3 5AB Bolton, U.K. He is now with the School of Engineering and the Built Environment, Edinburgh Napier University, EH10 5DT Edinburgh, U.K. (e-mail: c.see@napier.ac.uk).

Raed Abd-Alhameed is with the Faculty of Engineering and Informatics, University of Bradford, BD7 1DP Bradford, U.K. (e-mail: r.a.a.abd@bradford.ac.uk).

Francisco Falcone is with the Department of Electric and Electronic Engineering, Universidad Pública de Navarra, 31006 Pamplona, Spain (e-mail: francisco.falcone@unavarra.es).

Tayeb A. Denidni is with the Institut National de la Recherche Scientifique (INRS), Université du Quebec à Montréal, Montreal H2L 2C4, QC, Canada (e-mail: denidni@emt.inrs.ca).

Digital Object Identifier 10.1109/LAWP.2020.3010865

I. Introduction

RECENT technological advances have established possible the generation and discovery of Terahertz (THz) radiation [1–6]. This has resulted in a formerly inaccessible zone of the electromagnetic (EM) spectrum attainable, which is a territory of large potential for medical imaging and radio astronomy. Characteristics of the THz band permit it to occupy a unique niche as other parts of the EM spectrum are already well established [7]–[9]. One of the main obstacles encountered in realizing a commercial THz system is the high path loss and atmospheric attenuation incurred by the signal [10], [11]. This necessitates high-gain transmit and receive THz antennas. Typical THz antennas include a lens antenna, which is combined of an expanded hemispherical silicon lens [12], and a diagonal multilayer horn [13]. Although, these types of antennas provide high gain up to 12.5 dB; however, they are bulky structures that limits their applications.

In this letter, the viability of an on-chip antenna has been demonstrated to offer wide-frequency range and high-gain performance across 0.290–0.316 THz with a narrow stopband between 0.292 and 0.294 THz. High-gain performance is achieved by employing an aperture feed mechanism whereby THz EM energy is coupled from an open ended microstrip line via a metal slot-line to the radiation patch array with minimal loss. The antenna is fabricated on low permittivity THz substrate and on silicon technology. The proposed THz antenna for on-chip integration is simple to design and implement, and furthermore a low-profile structure.

II. Design Procedure of the On-Chip Antenna Excited With a Innovative Feeding Structure

Fig. 1 displays the 3-D vision of the proposed sub-THz on-chip antenna. The antenna includes of a periodic array of 15 radiating elements fabricated on the top surface of a polycarbonate layer. Each radiating element comprises a rectangular patch and a circular patch. Dimension of the rectangular patch is 2.8 × 0.2 mm^2, and the circular patch has a radius of 0.25 mm. Gap between the center of the two patches is 0.6 mm. Spacing between adjacent pairs of patches is 0.25 mm, which corresponds to the guided wavelength of the metal slot-line at 0.3 THz, thus ensuring the field distribution is uniform over the aperture of the antenna.

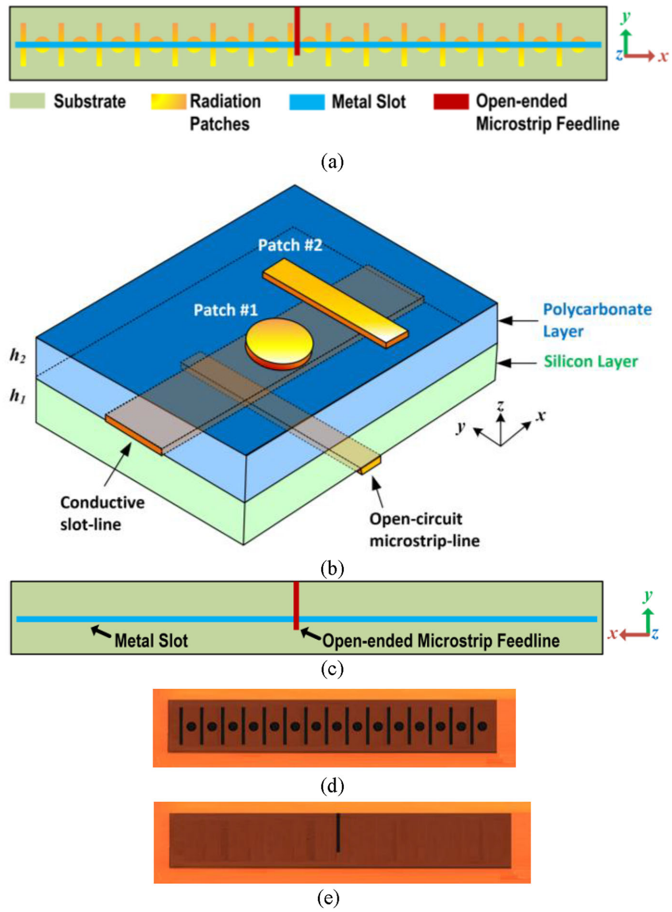

Fig. 1. Silicon-based integrated on-chip antenna. (a) Top-side. (b) Side-vision with a partially enlarged section. (c) Back view. (d) Manufactured prototype (top-side). (e) Manufactured prototype (bottom-side). The proposed on-chip antenna has a total dimension of $20 \times 3.5 \times 0.126$ mm^3. It is constructed from three different layers, i.e., polycarbonate, silicon, and aluminum.

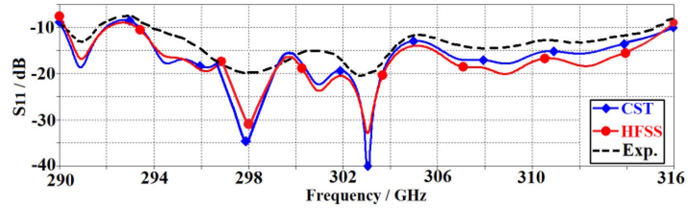

Fig. 2. Simulated and measured reflection coefficient ($S_{11} \leq -10$ dB).

The antenna array is fed serially through the open-circuited conductive slot-line with length and width of l = 19 mm and w = 0.16 mm, which is embedded in the high resistivity intrinsic silicon-substrate layer with a relative permittivity of ε_r = 11.9, tan δ = 0.00025, and a thickness of h_1 = 70 μm. Polycarbonate substrate is used to support the radiation patches. It has a relative permittivity of ε_r = 2.1, tan δ = 0.01, and a thickness of h_2 = 50 μm. The silicon and polycarbonate substrates were bonded together using thermal compression. Silicon is a low-thermal-expansion material; however, polycarbonate can experience thermal stresses during the annealing treatment which can induce fracturing in the polycarbonate substrate. It was found that by limiting the maximum annealing temperature the fracturing can be avoided. The metallization layer was created using sputter deposition process. The feed mechanism proposed here to excite the array is realized using an open-ended microstrip line which is implemented on the underside of the silicon layer and is orthogonally arranged relative to the metal slot-line. Dimensions of the open-circuited microstrip line are 2.8×0.2 mm^2. The conductive slot-line is embedded on the top surface of the silicon layer and is sandwiched between polycarbonate and silicon substrates to facilitate effective coupling of EM energy between the open-circuited microstrip line to the patch array. The radiation patches and open-ended microstrip line are made of Aluminum with conductivity of 3.8×10^7 S/m, thickness of 3 μm and surface roughness of 0.2 μm. Unlike previous antenna designs the proposed technique gets rid of the otherwise bulky structure. Parameters of the metal slot-line and radiation elements were optimized to match with the impedance of the feeding line in order to achieve high-gain performance over the antenna's sub-THz working band.

In the proposed on-chip antenna structure the travelling-wave propagating along the slot-line excites two orthogonal TM_{11} patch modes when the circular patch is placed on the aperture of the metal slot-line [14]. The two modes have a 90° phase difference because the phase of the electric field is 90° in advance of the current on a resonant patch [15]. As the amplitudes of the two modes are difficult to control it was necessary to include a linearly polarized rectangular patch. The combination of two different patches generates the required circularly polarized radiation. The phase and axial ratio of the two orthogonal modes can be controlled by adjusting two parameters, i.e., the spacing between adjacent pairs of patches and the open-circuit slot-line width.

The antenna's reflection coefficient ($S_{11} < -10$ dB) shown in Fig. 2 was determined with two different 3-D full-wave EM computational techniques (CST Microwave Studio & HFSS). The simulated and measured results show that, the proposed structure operates over the frequency range of 290–316 GHz for $S_{11} \leq -10$ dB, which corresponds to an impedance bandwidth of 8.5%. It is noticed that the antenna has a narrow stopband from 292 to 294 GHz, and there is excellent correlation observed between the two simulation tools. The empirical results in Fig. 2 verify the viability of the proposed THz antenna for wide-frequency range applications. The discrepancy observed between the measured and simulated results is due to: 1) the unknown dielectric loss tangent over the required frequency range in the foundry's design kit when the 3-D model of the antenna was constructed; 2) manufacturing tolerances; and 3) feed mismatch losses.

The simulated surface current distribution over the radiation elements at 300 GHz is shown in Fig.3 for different phase angles. It is evident that the rectangular-patches participate toward a

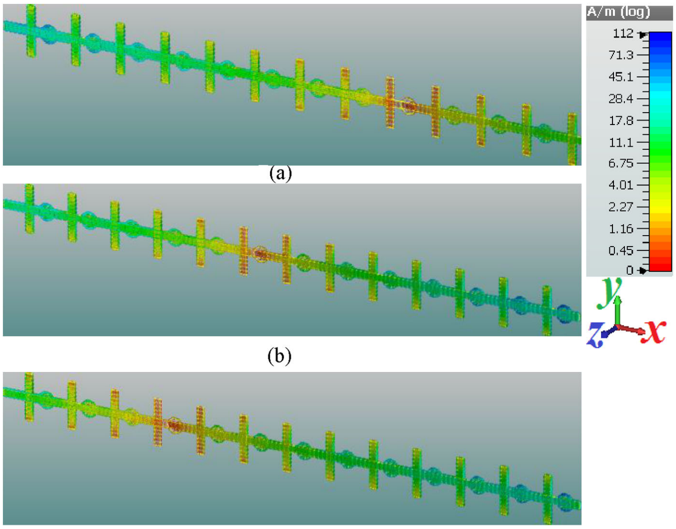

Fig. 3. Surface-current distribution over the radiation elements at 300 GHz for different phase angles: (a) 0°, (b) 90°, and (c) 270°.

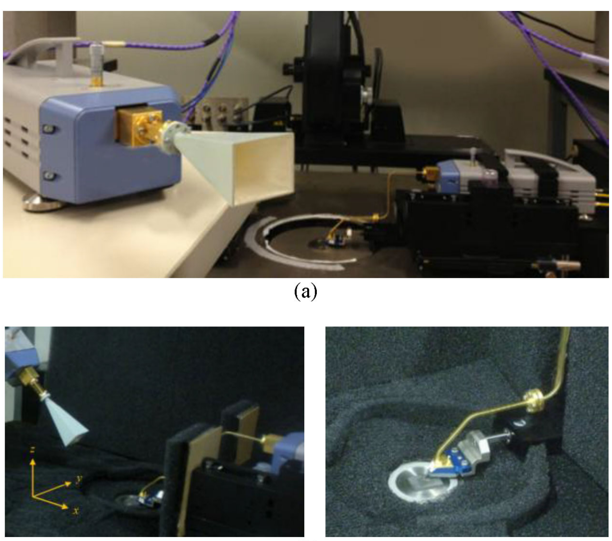

Fig. 4. (a) Sub-THz antenna measurement setup. (b) RF absorber material seen as black spongy sheets. The on-chip AUT was located on a Cascade Microtech rigid microwave absorber and probed applying the ground-signal-ground (GSG) RF probe. Physical contact was used to connect the ground pads of the GSG probe with the ground plane of the microstrip.

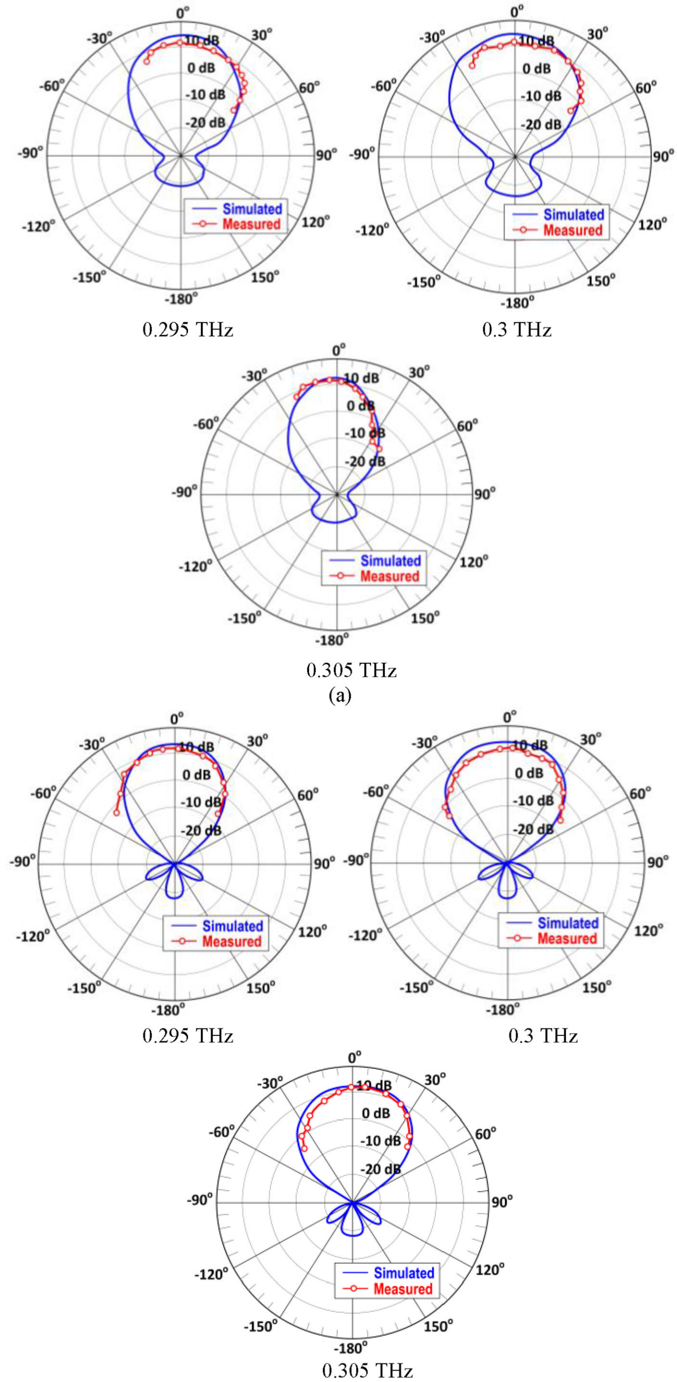

Fig. 5. Radiation patterns at 295, 300, and 305 GHz. (a) E-plane. (b) H-plane.

y-axis polarized radiation, and the circular patches participate toward both *x*- and *y*-axis polarizations, to yield left-handed circularly polarized radiation.

The antenna's radiation specifications were tested applying a compact antenna test range as illustrated in [16]. The antenna measurement setup with the attached horn antenna on the transmitter is shown in Fig. 4(a). To decrease multipath reflections in the test area, radio frequency (RF) absorbing material has utilized to nearly all metallic surfaces and objects on the probe station as shown in Fig. 4(b). A vacuum pump was used to hold down the chip to the rigid microwave absorber while the RF probe touched down. The actual measurements using the standard horn were made from below the antenna under test (AUT) in Fig. 4(b). *E*-and *H*-planes radiation patterns at the operating frequencies of 295, 300, and 305 GHz are plotted in Fig. 5(a) and (b), respectively. Axial-ratio *E*-plane of the THz antenna array at various spot frequencies across

TABLE I
MEASURED AXIAL-RATIO *E*-PLANE

Frequency (THz)	Axial-ratio E-plane
0.295	1.80
0.3	1.25
0.305	2.30

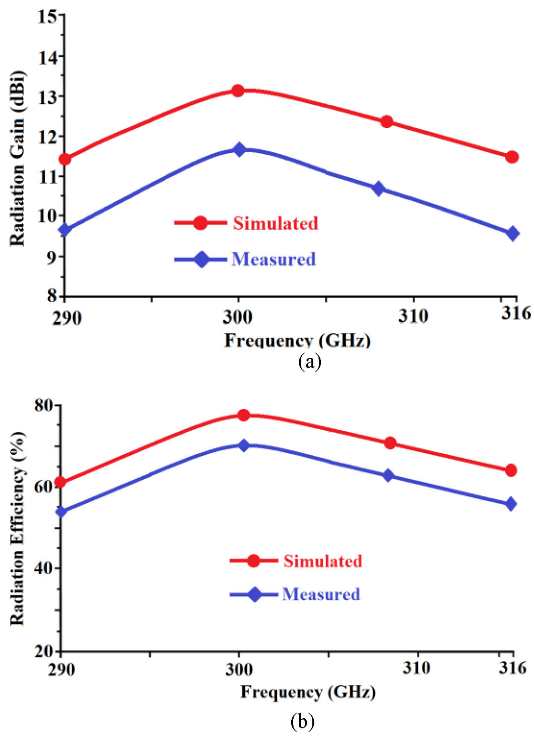

Fig. 6. (a) Gain. (b) Radiation efficiency as a function of frequency.

the antenna's working band are given in Table I. It shows the broadside axial ratio is maintained under 3 dB across the operating frequency range. Gain and radiation efficiency curves throughout the working frequency band are plotted in Fig. 6. The radiation efficiency was determined by taking the ratio of the measured radiated power to the input power. The measurement equipment of high thermal stability was carefully calibrated with highly accurate verification standards to minimize errors. Broadside gain and efficiency at 300 GHz are 11.71 dBi and 70.8%. Although, because of the characteristics of series fed antenna, when the operating frequency is away from 0.3 THz the beam is tilts slightly and the gain is marginally affected. The 3 dB bandwidth is shown to reduce at frequencies higher than 0.3 THz. The radiation gain and efficiency are also affected by the high conductor and dielectric loss at sub-THz band.

Performance parameters of the proposed silicon-based on-chip antenna has compared with recently published millimeter-wave antennas in Table II. It is evident that previous works are based on newer fabrication processes of 0.09, 0.13, and 0.18 μm technologies; however, in this letter the on-chip antenna was fabricated on a standard 120 μm process as the smallest dimension in the design is limited to 200 μm. The purpose of this investigation was to determine by how much we could extend the operating frequency range of a THz antenna using the standard silicon technology. Compared to the publications cited it exhibits a higher gain and radiation efficiency. Although, its radiation efficiency is lower than [23] that operates at 45–70 GHz; however, the proposed antenna works at a significantly higher frequency band of 290–316 GHz.

TABLE II
COMPARISON RESULTS

Ref.	Antenna Type	Meas. Freq. Band (GHz)	Meas. Gain (dBi)	Meas. Eff. (%)	Size (mm^3) or (mm^2)	Process
[17]	Bowtie-slot	90-105	$\leq$-1.78	-	0.71×0.3 1× 0.65	IHP 0.13-µm Bi-CMOS
[18]	Differential-fed Circularly Polarized	50-70	$\leq$-3.2	-	1.5×1.5 ×0.3	CMOS 0.18-µm
[19]	Ring-shaped Monopole	50-70	$\leq$0.02	$\leq$35	-	CMOS 0.18-µm
[20]	Circular Open-loop	57-67	$\leq$ -4.4	-	1.8×1.8 ×0.3	CMOS 0.18-µm
[21]	AMC embedded squared slot antenna	15-66	$\leq$ 2	-	1.44× 1.1	CMOS 0.09-µm
[22]	Monopole	45-70	$\leq$4.96	-	1.9×1.9× 0.25	Silicon CMOS
[23]	Loop Antenna	65-69	$\leq$8	$\leq$96	0.7× 1.25	CMOS 0.18-µm
[24]	Dipole-Antenna	95-102	$\leq$4.8	-	-	Bi-CMOS
[25]	Tab Monopole	45-75	$\leq$0.1	$\leq$42	1.5×1	Standard CMOS Silicon
This letter	Coupled Feeding Mechanism	290-316	$\geq$9.6	$\geq$55	20×3.5×0 .126	Standard 120-µm Silicon

III. CONCLUSION

Feasibility of an on-chip antenna model is investigated for sub-THz applications. The antenna model is implemented on silicon technology for easy on-chip integration. The antenna employs aperture fed mechanism comprising an open-circuited microstrip line that is electromagnetically coupled to an orthogonal metal slot-line and periodic array of radiating elements. The proposed on-chip antenna with small dimensions of $20 \times 3.5 \times 0.126$ mm^3 operates across 0.290 to 0.316 THz with an optimum gain of 11.71 dBi and radiation efficiency of 70.8% at 0.30 THz, and it radiates circularly polarized energy. The antenna has a narrow stopband between 0.292 and 0.294 THz.

REFERENCES

[1] S. S. Dhillon *et al.*, "The 2017 terahertz science and technology roadmap," *J. Phys. D. Appl. Phys.*, vol. 50, no. 4, 2017, Art. no. 043001.

[2] T. Nagatsuma *et al.*, "Advances in terahertz communications accelerated by photonics," *Nature Photon.*, vol. 10, pp. 371–379, 2016.

[3] I. F. Akyildiz *et al.*, "Terahertz band: Next frontier for wireless communications," *Phys. Commun.*, vol. 12, pp. 16–32, 2014.

[4] H. J. Song and T. Nagatsuma, "Present and future of terahertz communications," *IEEE Trans. THz Sci. Technol.*, vol. 1, no. 1, pp. 256–263, Sep. 2011.

[5] Y. Shimada, H. Iida, and M. Kinoshita , "Recent research trends of terahertz measurement standards," *IEEE Trans. THz Sci. Technol.*, vol. 5, no. 6, pp. 1166–1172, Nov. 2015.

[6] R. Al Hadi *et al.*, "A 1k-pixel video camera for 0.7-1.1 terahertz imaging applications in 65-nm CMOS," *IEEE J. Solid-State Circuit*, vol. 47, vol. 12, pp. 2999–3012, Dec. 2012.

[7] G. W. Hanson, "Radiation efficiency of nano-radius dipole antennas in the microwave and far-infrared regimes," *IEEE Antenna Propag. Mag.*, vol. 50, no. 3, pp. 66–77, Jun. 2008.

[8] D.-K. Lee, "Highly sensitive and selective sugar detection by terahertz nano-antennas," *Sci. Rep.*, vol. 5, 2015, Art. no. 15459.

[9] C. Feuillet-Palma *et al.*, "Strong near field enhancement in THz nano-antenna arrays," *Sci. Rep.*, vol. 3, 2013, Art. no. 1361.

[10] M. Tamagnone *et al.*, "Analysis and design of THz antennas on plasmonic resonant Graphene sheets," *J. Appl. Phys.*, vol. 112, no. 11, 2012, Art. no. 114915.

[11] M. Dragoman *et al.*, "Terahertz antenna based on graphene," *J. Appl. Phys.*, vol. 107, no. 10, 2010, Art. no. 104313.

[12] N. Llombart *et al.*, "Silicon micromachined lens antenna for THz integrated heterodyne arrays," *IEEE Trans. THz Sci. Technol.*, vol. 3, no. 5, pp. 515–523, Sep. 2013.

[13] W. Hou, Z.-Y. Sun, Y.-f. Jiang, Y. Liu, and X. Lv, "A terahertz diagonal multilayer horn antenna based on MEMS technology," in *Proc. IEEE MTT-S Int. Microw. Workshop Ser. Adv. Mater. Processes RF THz Appl.*, 2015, pp. 1–3.

[14] H. Yi, S.-W. Qu, and X. Bai, "Antenna array excited by spoof planar plasmonic waveguide," *IEEE Antennas Wireless Propag. Lett.*, vol. 13, pp. 1227–1230, 2014.

[15] J. R. James and P. S. Hall, *Handbook of Microstrip Antennas*, London, U.K: Institution Eng. Technol. 1989.

[16] C. Liu and X. Wang, "Design and test of a 0.3 THz compact antenna test range," *Prog. Electromagn. Res. Lett.*, vol. 70, pp. 81–87, 2017.

[17] M. S. Khan *et al.*, "Design of bowtie-slot on-chip antenna backed with E-shaped FSS at 94 GHz," in *Proc. 10th Eur. Conf. Antennas Propag.*, 2016, pp. 1–3.

[18] L. Wang and W. Z. Sun, "A 60-GHz differential-fed circularly polarized on-chip antenna based on 0.18-m COMS technology with AMC structure," in *Proc. IET Int. Radar Conf.*, 2015, pp. 1–4.

[19] H. T. Huang, Bo Yuan, X. Hong Zhang, Z. Fang Hu, and G. Qing Luo "A circular ring-shape monopole on-chip antenna with artificial magnetic conductor," in *Proc. IEEE Asia-Pacific Microw. Conf.*, 2015, pp. 1–3.

[20] X. Y. Bao, Y.-X. Guo, and Y.-Z. Xiong, "60-GHz AMC-based circularly polarized on-chip antenna using standard 0.18m CMOS technology," *IEEE Trans. Antenna Propag.*, vol. 60, no. 5, pp. 2234–2241, May 2012.

[21] F. Lin and B. L. Ooi, "Integrated millimeter-wave on-chip antenna design employing artificial magnetic conductor," in *Proc. IEEE Int. Symp. Radio-Freq. Integration Technol.*, 2009, pp. 174–177.

[22] S. Upadhyay and S. Srivastava, "A 60-GHz on-chip monopole antenna using silicon technology," in *Proc. IEEE Appl. Electromagn. Conf.*, 2013, 1–2.

[23] Y. Song, Y. Wu, J. Yang, and K. Kang, "The design of a high gain on-chip antenna for SoC application," in *Proc. IEEE MTT-S Int. Microw. Workshop Ser. Adv. Mater. Processes RF THz Appl.*, 2015, 1–3.

[24] M. Nafe, A. Syed, and A. Shamim, "Gain enhancement of low profile on-chip dipole antenna via artificial magnetic conductor at 94 GHz," in *Proc. 9th Eur. Conf. Antennas Propag.*, 2015, pp. 1–3.

[25] W. Yang, K. Ma, K. Seng Yeo, and W. Meng Lim, "A 60 GHz on-chip antenna in standard CMOS silicon Technology," in *Proc. IEEE Asia Pacific Conf. Circuits Syst.*, 2012, pp. 252–255.